Classification of ponds from high-spatial resolution remote sensing: Application to Rift Valley Fever epidemics in Senegal

J.P. Lacaux [a], Y.M. Tourre [a,1], C. Vignolles [a,*], J.A. Ndione [b], M. Lafaye [c]

[a] Médias-France, Toulouse, France, 18 avenue Edouard Belin — Bpi 2102, 31401 Toulouse Cedex 9, France
[b] Centre de Suivi Ecologique (CSE), Laboratoire de Physique de l'Atmosphère et de l'Océan Siméon Fongang (LPAO-SF), Dakar, Sénégal
[c] Centre National d'Etudes Spatiales (CNES), Toulouse, France

Abstract

During the rainy season the abundance of mosquitoes over the Ferlo region (Senegal) is linked to dynamic, vegetation cover and turbidity of temporary and relatively small ponds. The latter create a variable environment where mosquitoes can thrive and thus contribute to diffusion and transmission of diseases such as the Rift Valley Fever (RVF, with *Aedes vexans arabiensis* and *Culex poicilipes* mosquitoes) in the Ferlo. The small size and complex distribution of ponds require the use of high-spatial resolution satellite images for adequate detection. Here the use of SPOT-5 images (10 m-resolution) allows for detailed assessment of spatio-temporal evolution of ponds, through two new indices: i.e., the Normalized Difference Pond Index (NDPI), and the Normalized Difference Turbidity Index (NDTI). Small ponds less than 0.5 ha dominate whatever the time period. For example they represent nearly 65% of the total ponds during the peak of the rainy season, up to 90% at the end of the same season. Moreover, another product is proposed: the Zone Potentially Occupied by Mosquitoes (ZPOM). During the apex of the summer monsoon, it is found that RVF mosquitoes occupy 25% of the Ferlo region, while only 0.9% of the same area is covered by ponds. Overlapping areas occupied by grazing cattle and mosquitoes, enhance RVF virus transmission. The remotely sensed operational indices and products presented here are meant to better understand the mechanisms at stake and to contribute to the development of early warning systems in a changing climate and environment.
© 2006 Elsevier Inc. All rights reserved.

Keywords: Remote sensing, Rift Valley Fever; Ponds; *Aedes*; *Culex*; Senegal

1. Introduction

Over East Africa, climate ensemble forecasting technique may provide early warning of malaria risks in prone regions (Thomson et al., 2006). In general, higher than average seasonal rainfall should lead to increased cases of malaria. Linkages between rainfall and Rift Valley Fever (RVF) epidemics have also been highlighted by Linthicum et al. (1999) using the Normalized Difference Vegetation Index (NDVI) as a proxy for rainfall (Anyamba & Tucker, 2005; Tucker & Nicholson, 1999). Anyamba et al. (2001) have also studied relationships between

RVF occurrence, interannual variability of the warm phase of El Niño-Southern Oscillation (ENSO), and excess rainfall over Kenya.

In West Africa and over Senegal and southern Mauritania, RVF epidemics (Diallo et al., 2005), do not seem to follow the same relationships as over East Africa. The spatio-temporal distribution of discrete rainfall events (such as squall lines) during the rainy/summer monsoon season (contrary to the seasonal amount of total rainfall over East Africa) appears to be the confounding parameter for mosquitoes' production (see Ndione et al., 2003). This is particularly true for the *Aedes vexans* mosquitoes whose eggs are often laid along the edges of the ponds. When the time lags between two rainfall events is large (∼10 to 15 days), the number of eggs present along the dried-up ponds' edges becomes quite important. Intense rainfall events (i.e., more than 20 mm, as produced by squall lines),

* Corresponding author. Tel.: +33 5 61 27 37 23; fax: +33 5 61 28 29 05.
E-mail addresses: jean-pierre.lacaux@medias.cnes.fr (J.P. Lacaux), cecile.vignolles@medias.cnes.fr (C. Vignolles).
[1] Y.M. Tourre, LDEO of Columbia University, Palisades, NY, USA.

become thus triggering and powerful mechanisms for enhanced hatching (see also Mondet et al., 2005a,b). Recently, modeling results by Porphyre et al. (2005) linking ponds' dynamics, discrete rainfall events, and mosquitoes' abundance involved with RVF, have been successfully implemented.

Moreover, the mosquitoes' abundance and species seem to be a function of vegetation cover and turbidity within ponds (Bâ et al., 2005; Chevalier et al., 2004, 2005; Mondet et al., 2005b). Shallow ponds are declared turbid when they may become muddy on occasions due to rainfall events and use by local cattle. These muddy conditions can be short-lived, but at times a pond will become so well-mixed that it will fail to clear and stay turbid. Turbidity is caused by particles (typically clay with suspended organic/non-organic elements, including algae). In our case, turbidity is also a function of intensive domestic use from nearby villages. Overall turbidity is a measure of suspended sediments. According to Mondet et al., *Aedes vexans* lay eggs on ponds' edges with or without vegetation. Moreover the adult *Aedes* may use vegetation within ponds as resting heavens (Chevalier et al., 2005). The latter conditions favor reproductive amplification and diffusion of the RVF. This is particularly true at the end of the rainy season (Bâ et al., 2005). Concerning turbidity, *Culex poicilipes* and *A. vexans*, both prefer an environment with clear and free waters, for laying eggs (Beaty & Marquardt, 1996; Bicout, 2001).

From the above, a new approach using high-spatial resolution images from space, for ponds' detection and classification is being proposed. The area under investigation is the Ferlo region (Senegal) centered over the populated village of Barkedji (15°16'46″N, 14°52'5″W, Fig. 1). It belongs to the Sahelian savannah ecological zone, where recent studies on the RVF have been conducted, (i.e., Chevalier et al., 2004; Mondet et al., 2005b; Ndione et al., 2003; Traoré-Lamizana et al., 2001, among others). The main and original result was that the spatio-temporal distribution of rainfall, ponds' dynamics with their vegetation cover and turbidity, are all closely linked with the production of mosquitoes associated with RVF.
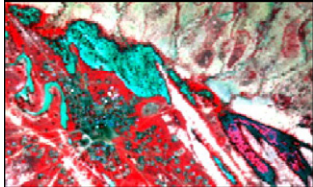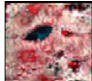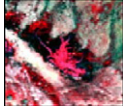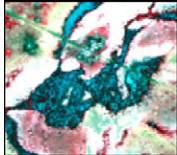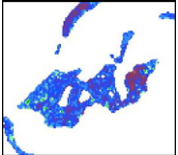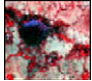
Here the climate is typically Sahelian with a summer monsoon (the rainy season) from July to mid-October. During that period the region is also under the influence of maritime influence from the deflected trade-winds and water-vapor advection from the eastern Atlantic Ocean (Jarlan et al., 2005; Moron, 1994). Overall, the mean annual rainfall there is mainly provided by squall lines, and ranges from 300 mm to 500 mm (Nicholson, 1979). During the summer monsoon, a large quantity of small and temporary ponds are thus formed leading to an environment favoring mosquitoes' breeding and hatching, including *A. vexans arabiensis* and *C. poicilipes* associated with the RVF (Bâ et al., 2005; Fontenille et al., 1998). Contemporaneously, human and/or grazing live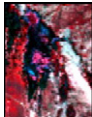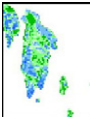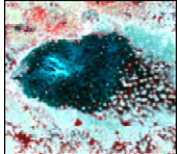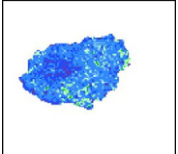stock from the relatively lush area are exposed to several vector borne diseases such as RVF, Malaria, West Nile, and Japanese Encephalitis, among others. Thus seasonal ponds are seen as key places where cattle and vectors do meet, and as such become potent sources for epidemics. In the Ferlo region, ponds are widely distributed, some isolated, and others organized in clusters of all sizes. Different types of ponds exist with different level of vegetation cover inside and different degrees of turbidity. Vegetation cover includes embedded trees such as *Acacia sp.*, *Mytragena inermis*, *Diospyros mespiliformis* and *Balanites aegyptiaca*, annual herbaceous plants such as *Oryza barthii* (wild rice), *Cassia obsutifolia*, *Eragrostis tremula* and *Schoenefeldia gracilis*, and floating vegetation such as *Cenatotheca sesamoïdes* (water-lilies). In this study, seven ponds have been selected for their specific characteristics. Their selection depended also upon the availability of contingent in-situ multidisciplinary datasets: entomology, virology, hydrology, meteorology, land cover, among others. The seven ponds are: Barkedji, Furdu, Kangaledji, Loumbel Lana, Ngao, Niaka and Yaralope. Physical characteristics of these ponds are presented in Table 1, using ground survey by Ndione from CSE (this study) and Chevalier et al. (2004, 2005).
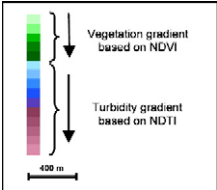
In this paper the blend of in-situ data and local observation with images and datasets obtained from remote sensing permit to produce detailed mapping of variable environmental

Fig. 1. Map of Senegal in West Africa from Atlas of Africa (Jaguar Edit.). The small red square outlines the studied area, covered with ponds, and within the Ferlo region.

Table 1
The seven ponds in the Ferlo region under investigation

Pond's name and localisation	Characteristics	False color composite	Classification of ponds
Barkedji (15°17N, 14°52W)	Large pond (several hectares), deep (maximum depth 1.7 m), very turbid and poor in vegetation, inside Ferlo bed		
Furdu (15°15′21″N, 14°51′38″W)	Small pond (less than 2 ha), not deep (maximum depth 0.7 m), slightly turbid and rather rich in vegetation, outside Ferlo bed		
Kangaledji (15°16′25″N 14°50′40″W,)	Pond of intermediate size, less turbid than Barkedji and very rich in vegetation, inside Ferlo bed		
Loumbel Lana (15°15′25″N, 14°43′6″W)	Large pond (several hectares), with intermediate depth (maximum depth 1.2 m), slightly turbid, poor in vegetation, inside Ferlo bed		
Ngao (15°14′30″N, 14°51′5″W)	Pond of intermediate size, not very deep, (maximum depth 0.8 m), less turbid than Barkedji and rich in vegetation, outside Ferlo bed		
Niaka (15°17′46″N, 14°53′56″W)	Pond of intermediate size, with intermediate depth (maximum depth 1.2 m), less turbid than Barkedji, very rich in vegetation, inside Ferlo bed		
Yaralope (15°21′43″N, 14°48′38″W)	Large pond (several hectares), with intermediate depth (maximum depth 1m), less turbid than Barkedji, poor in vegetation, outside Ferlo bed		

The left column is geo-referencing and name of each pond. The second column (from left) is for qualitative description (size, vegetation over, depth, turbidity) of the same ponds based upon in-situ surveys. The third column (from left) is for classic false color composite obtained from SPOT-5 images and for the same ponds. Right column: degrees of vegetation cover and turbidity within the same ponds.

conditions– ponds dynamics, vegetation cover, turbidity– associated with mosquitoes' production and abundance.

2. Data and methodology

From remotely sensed high-spatial resolution images and datasets, derived indices and products are presented. Indices are mainly used to locate and classify ponds in the Ferlo region (Senegal), as a function of vegetation invasion and degrees of turbidity.

2.1. Images and data

In order to outline ponds' contours in great details and detect small ponds (i.e., down to 0.1 ha, and which are numerous in the investigated zone), SPOT-5 multi-spectral high-spatial resolution images (10-m), had to be used. Pre-processed 'Level 2A' images (http://www.spotimage.com.cn/spot5/ensavoirplus/eng/plus_niveau.html) are first retrieved. The 'digital counts' (DCs hereafter) include radiometric and geometric corrections, while atmospheric effects and effects from variable viewing angles are not taken into
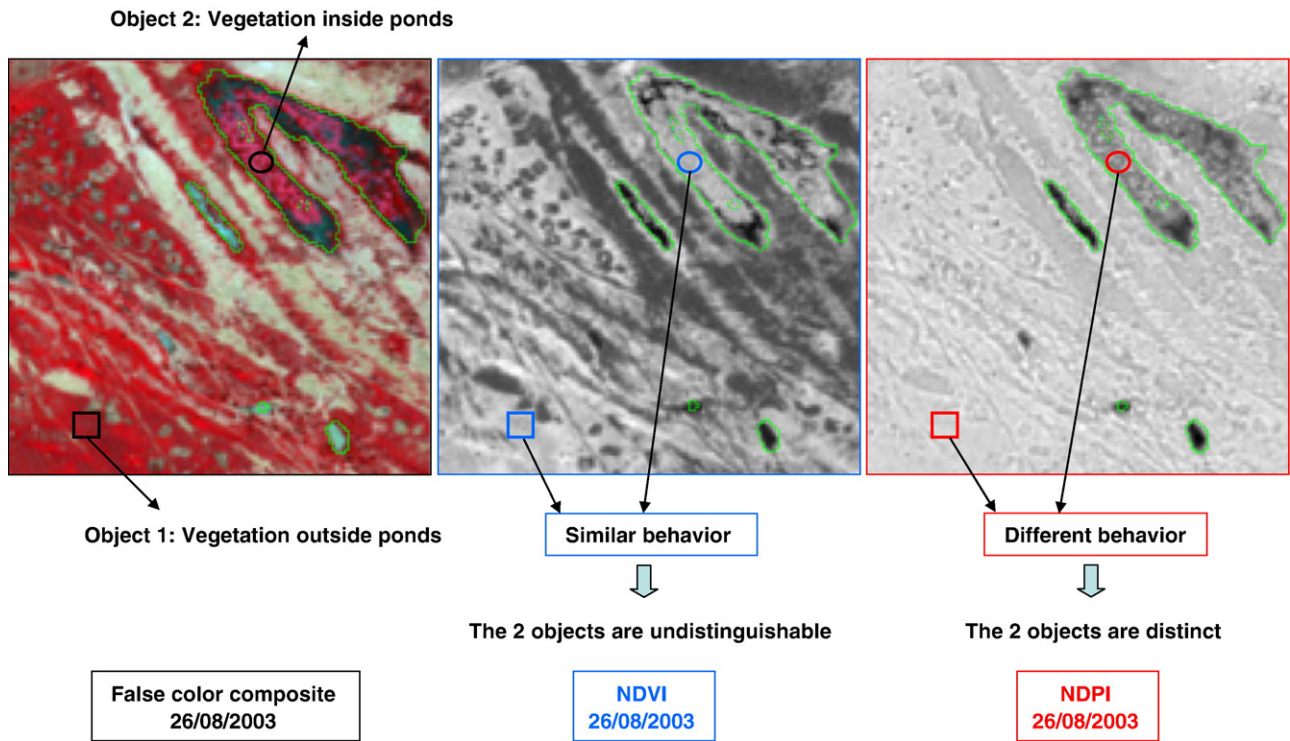
Object 2: Vegetation inside ponds

Object 1: Vegetation outside ponds

Similar behavior ⇩ The 2 objects are undistinguishable

Different behavior ⇩ The 2 objects are distinct

False color composite 26/08/2003

NDVI 26/08/2003

NDPI 26/08/2003

Fig. 2. Detection of ponds — comparison between the 'classic' NDVI index and the new NDPI index.

account. Four spectral bands have been used to compute the different indices presented hereafter: The wavelengths for the four bands are defined as follows:

– green: 0.50–0.59 μm,
– red: 0.61–0.68 μm,
– near infrared (or NIR, hereafter): 0.78–0.89 μm
– middle infrared (or MIR, hereafter): 1.58–1.75 μm

Each image covers an area of ∼ 3600 km^2 (60 km × 60 km), centered over the village of Barkedji. The dates for the five processed images are: August 26th, 2003: peak of the rainy season; October 17th and 27th, 2003: end of the rainy season; and November 18th, 2003 and January 19th, 2004: heart of the dry season.

Relative geo-referencing for all images and adjustment to minimize spatial errors are based upon the first image taken as the 'reference level'. Polynomial warping, and re-sampling methods such as nearest neighbor values, bilinear and/or cubic convolutions were tested and evaluated when compared to ground-controlled checkpoints. The best results were obtained by using cubic convolution. In our study, the average RMS is 0.3 pixel which is below the generally accepted precision of an averaged RMS of one pixel (Bonn & Rochon, 1996).

2.2. Methodology: detection and classification of ponds

2.2.1. Detection of ponds

As explained by Puech (1994), detecting water bodies including ponds, has been accomplished through the use of either different indices such as the Normalized Difference

Vegetation Index (or NDVI hereafter) following (Rouse et al., 1973; Tucker, 1979) or spectral band ratios such as NIR/Red and Red/Green. The above ratios allowed also for clear distinction between water bodies from different types of ground cover.

Here the use of 'classic index' such as the NDVI did not perform well enough when results were compared to ground-truth observations. For example in Fig. 2, it should be noted that in the classic NDVI image, the behavior of vegetation inside and outside of ponds cannot be distinguished. Thus the latter index cannot be used for detecting vegetation within pond, which is not the case with the new NDPI (see right panel of Fig. 2). Thus, a new index for remote sensing of small and temporary ponds has been derived: the so-called Normalized
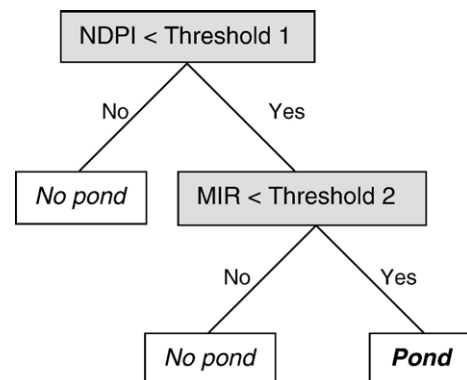

Fig. 3. Detection of ponds using a simple decision-tree classifier. Threshold 1, based upon a new index, or NDPI, allows for detection of ponds including water, vegetation and suspended materials plus some types of soils. Threshold 2, based upon the middle infrared (or MIR) digital counts (DCs), allows for identification of ponds only.
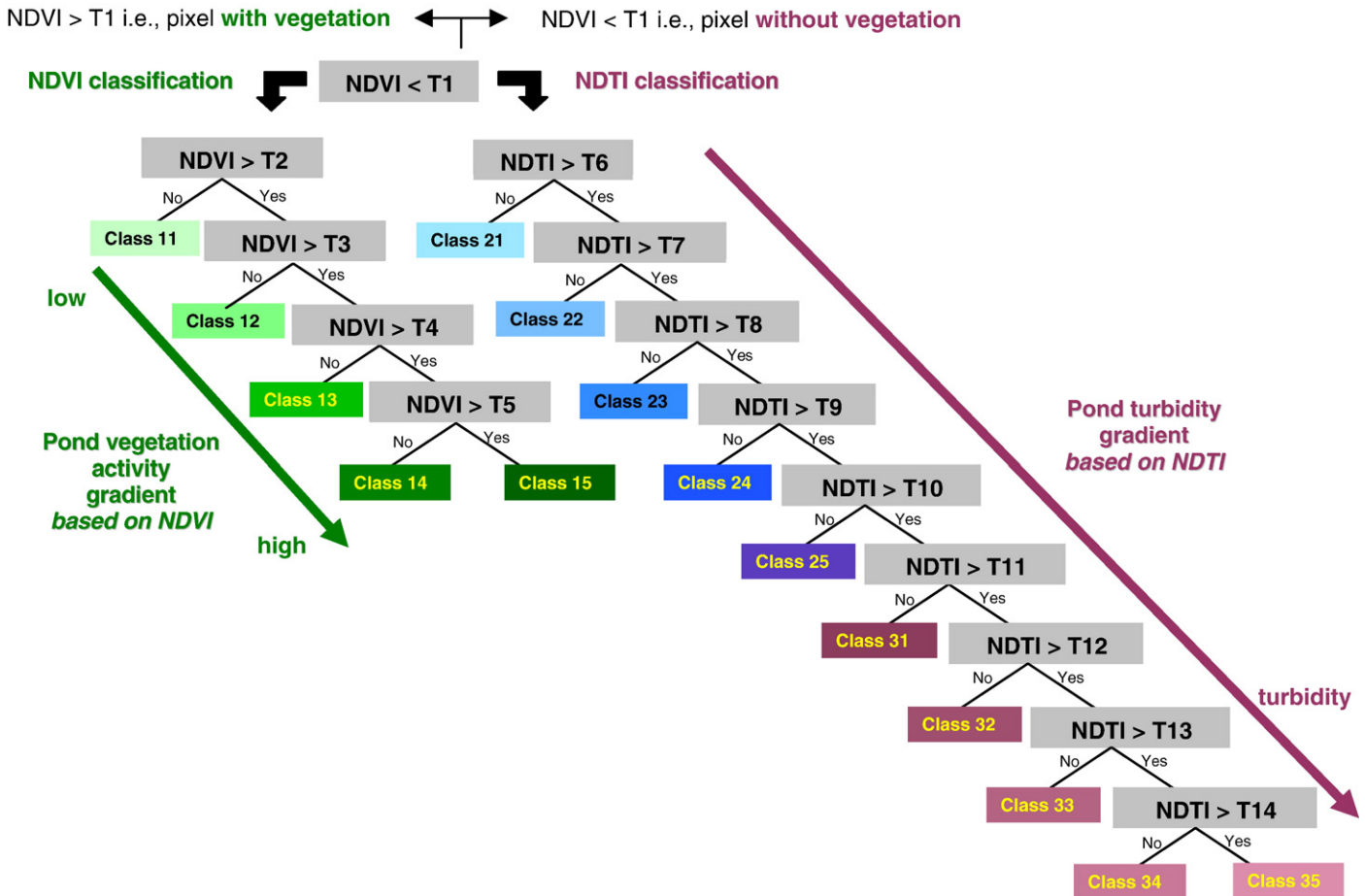
Fig. 4. Classification of ponds using a more complex decision-tree classifier. T_1 is an NDVI threshold to distinguish pixels within ponds with or without vegetation. The slanted green arrow corresponds to NDVI thresholds (T_2 to T_5) associated with vegetation gradient. The slanted burgundy arrow corresponds to NDTI thresholds (T_6 to T_{14}) associated with turbidity gradient.

Difference Pond Index (or NDPI, hereafter). The NDPI combines the digital counts (DCs) for the MIR and green bands of the electromagnetic spectrum, as follows:

$$NDPI = (DCs_{mir} - DCs_{green})/(DCs_{mir} + DCs_{green})$$

DCs correspond to radiometric values for each specific band and each individual pixel.

Ponds' mapping is produced through manual photointerpretation from in-situ photography for the seven ponds under investigation. Throughout photointerpretation techniques, thresholds for the NDPI were identified for each image. This allowed for detailed sorting between ponds and different types of soils. Since different types of soils induce different MIR responses, threshold values were thus applied only to the MIR spectral band for each image. Images were then sorted according to identified thresholds for both NDPI and MIR, using the decision-tree conditional classifier (see Fig. 3). The latter analytical tool allows for multi-stage classification by using series of binary decisions for pixels' sorting. Each single decision partitions pixels into subsets of two-class images. Each subset is based upon its own logical mathematical function. Thresholds for NDPI and MIR may vary from date to date, due

to different atmospheric effects and viewing conditions. It is found here, that the NDPI makes it possible not only to distinguish small ponds and water bodies (down to 0.01 ha), but also to differentiate vegetation inside ponds from that in their surroundings.

2.2.2. Classification of ponds

Classification of ponds is performed from their vegetation cover and degrees of water turbidity. These two parameters condition mosquitoes' behavior (i.e., reproduction, abundance...). The NDVI makes it only possible to identify vegetation which a given chlorophyllian activity. It is a robust indicator for density and vigor of green vegetation, (Guyot & Seguin, 1988; Tucker, 1979). After detecting ponds' contours and their spatial coverage, ponds with/without vegetation, ponds with different degrees of turbidity were also sorted-out. As an example in order to show how the seven ponds were classified, compilation for the August 26th, 2003 scene is given in Table 1. The percentage of vegetation invasion inside ponds is obtained by using NDVI and combining DCs of NIR and red bands of the electromagnetic spectrum, as follows:

$$NDVI = (DCs_{nir} - DCs_{red})/(DCs_{nir} + DCs_{red})$$

Table 2
Percentage of ponds coverage for the Ferlo region (for the same period), also given in hectares

Date	Ponds' percentage	Ponds' area (in ha)	Number of ponds
August 26th, 2003	0.9	1703	1354
October 17th, 2003	0.1	199	310
October 27th, 2003	0.09	172	727
November 18th, 2003	0.03	60	236
January 19th, 2004	0.01	9	29

The first column is for dates, while the associated number of ponds is found in the last column.

Then through photointerpretation, thresholds of NDVI were known when vegetation was found (or not found), within ponds' limits. Once the percentage of vegetation inside the ponds was determined, the remnant of ponds without vegetation was analyzed to estimate different degrees of turbidity. This lead to a new index: the Normalized Difference Turbidity Index (or NDTI hereafter) which combines DCs of the red and green bands of the electromagnetic spectrum, as follows:

$$NDTI = (DCs_{red} - DCs_{green})/(DCs_{red} + DCs_{green})$$

Pure water has a specific radiometric response: its DC while weak in the green wavelength (less than 10%), becomes very small in the red wavelength and quasi-null in the near infrared (Robin, 1995). When, water bodies such as small ponds are used for domestic and cattle needs, they become muddy and loaded with suspended sediments. The increase turbidity and its associated radiometric responses make the pond behave like bared soils (Guyot, 1989). However, since the values of the red radiometric responses are much larger than that of the green ones, the relationship between the green and the red wavelengths is reversed (Campbell, 1996; Verbyla, 1995). Images are then sorted-out from both NDVI and NDTI thresholds and by using once more a decision-tree conditional classifier (see Fig. 4).

Finally, statistics are obtained for each individual pond, after classification and polygonal vectorization. Remotely sensed data is then carefully crossed with actual pictures of ponds.

3. Results

During the peak of the rainy season (August 26th, 2003), the significant number of ponds is of 1354 (Table 2). This represents 1703 ha or 0.9% of the total area of the investigated zone (198, 300 ha). At the end of the rainy season, around October 17th, 2003, the surface occupied by ponds fell by almost 88% (i.e., ~ 199 ha). This is a 'classic' behavior induced by the dynamics of temporary ponds in the Sahelian region. In the midst of the dry season almost all ponds have disappeared leaving 9 ha occupied by only 29 ponds.

In Fig. 5, the evolution of the ponds distribution according to their surface is displayed. Ponds of small size (less than 0.5 ha) dominate whatever the time. They represent for example nearly 65% of the detected ponds during August 26th, 2003. The presence of these numerous small ponds highlights the needs of high-spatial resolution remote sensing. This allows for detection of small ponds (down to 0.01 ha).

The use of several images during the same rainy season and then during the following dry season, enables to quantify ponds' dynamics. As an example the dynamic of Barkedji's pond is displayed in Fig. 6. The progressive drying-out of the pond can be seen, as a function of time.

From both NDVI and NDTI the seven ponds of reference have been sorted-out. During August 26th, 2003, adequate matching could be found between false color compositing and the ponds' classification (Table 1). The false color compositing was obtained by associating red color and NIR wavelengths, green color and red wavelengths, and blue color and green wavelengths, respectively. However the vegetation with photosynthetic activity has a reflectance in the NIR range well superior than that in the visible domain (Guyot & Seguin, 1988). The vegetation appears then in red when using false color compositing. It should be noted that pixels belonging to
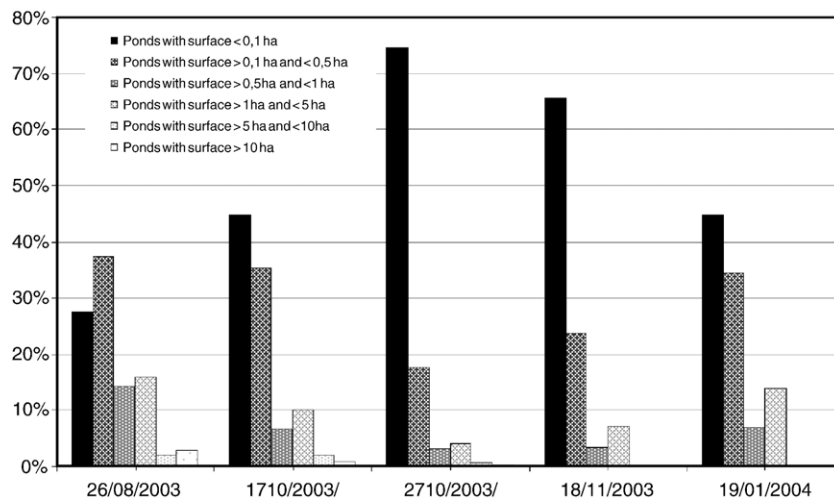

Fig. 5. Distribution and evolution of ponds as a function of time (from summer 2003 to beginning of winter 2004). Abscissa axis is for the SPOT-5 images dates. Ordinate axis is for percentage of ponds with given size limits. Shadings represent the six classes for ponds' sizes.
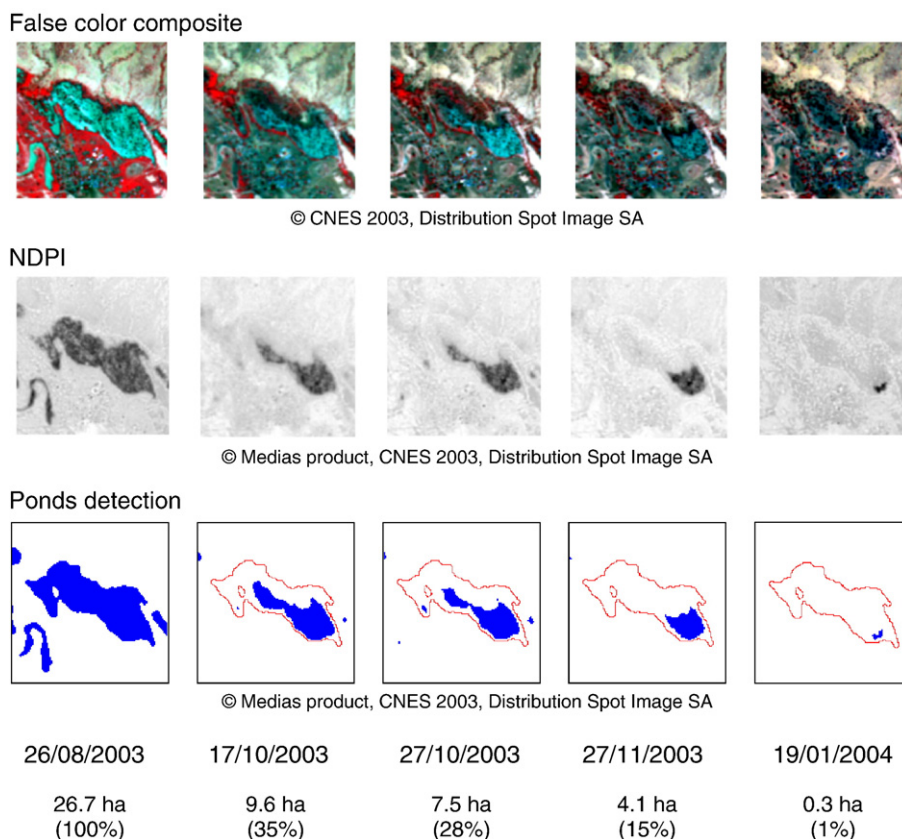
Fig. 6. An example of the dynamic for the Barkedji pond during the same period as in Fig. 5. Top: Classic false color composite from SPOT-5 images over the Barkedji zone. Red is for near infrared (NIR). Middle: NDPI for the Barkedji zone. Darker areas are for ponds (i.e., small values of NDPI). Bottom: Detailed detection of ponds for the Barkedji zone in hectares. The rate of draining is expressed in %. The red outline is for the pond's contour during the peak of the rainy season.

ponds and which appear in red in the false color compositing have been correctly identified as vegetation. The false color compositing reveals that pixels belonging to extreme turbid water appear with the cyan color (see the Barkedji pond as an example). Pixels inside ponds with a cyan appearance from false color compositing were correctly linked to the turbid water category within ponds.

Statistics for the seven ponds were then computed to evaluate percentage of vegetation, turbid/non-turbid water within ponds

Table 3
Detailed statistics for the studied seven ponds

Ponds' name	Pond's surface (in ha)	Vegetation cover (in %)	Free water (in %)	
			non-turbid	turbid
Barkedji	26.7	8%	12%	80%
Furdu	1.6	28%	72%	0%
Kangaledji	10.3	79%	21%	0%
Loumbel Lana	26.4	7%	87%	6%
Ngao	4.0	37%	63%	0%
Niaka	12.6	60%	40%	0%
Yaralope	34.3	11%	89%	0%

Names of ponds are in the left column, their respective areas are in the second column. Associated vegetation cover (in %) is found in the third column. The last two columns are for percentages of non-turbid/turbid free water within ponds.

(see Table 3). The Barkedji's pond is ∼80% turbid with less than ∼10% vegetation at its surface. On the contrary, Kangaledji and Niaka ponds are heavily vegetated (79% and 60% of vegetation coverage, respectively). The Loumbel Lana, Barkedji and Yaralope ponds have little vegetation (7%, 8%, and 11% of pixels, respectively). Finally, vegetation covers of the Nago and Furdu ponds are more important than those of Barkedji, Loumbel and Yaralope ponds but less important than those of Kangaledji and Niaka ponds.

From the turbidity testing Barkedji is classified as very turbid (80%), whereas the others ponds display little or no turbidity (i.e., less than 10% of pixels).

It was thus possible, by using the above new indices, to determine for each pond and with some accuracy, percentage of vegetation cover as well as relative percentages of turbid/clear water. It is recognized that additional testing and field recognition are required to estimate the actual levels of accuracy.

4. Discussion and conclusion

In the recent literature and latest results on mosquitoes' abundance and RVF diffusion over the Ferlo region, it becomes clearer that the spatio-temporal variability of rainy events is of the utmost importance. That variability control ponds' dynamic, invasion of vegetation, and degrees of turbidity of ponds, and is more important than seasonal rainfall as a whole (Chevalier

Ponds' map (26/08/2003) ZPOM (26/08/2003)

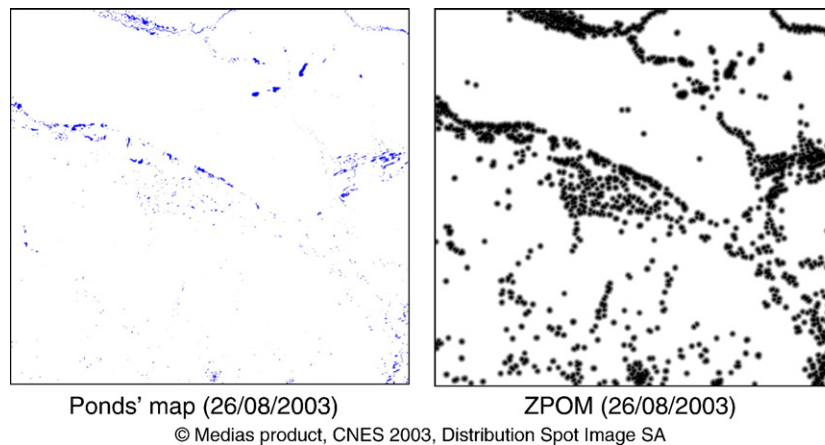© Medias product, CNES 2003, Distribution Spot Image SA

Fig. 7. The new ZPOM index for the Ferlo region. Left: Ponds detected during the peak of the rainy season. Clusters of ponds can be easily identified. Right: Associated zone potentially occupied by mosquitoes during the same time, following Bâ et al. (2005).

et al., 2005; Mondet et al., 2005b; Ndione et al., 2003; Porphyre et al., 2005, among others). In turn, behavior and habits of *Aedes* and *Culex* RVF mosquitoes depend also upon the variability of the latter ponds' parameters and local environmental conditions. A detailed classification at the ponds' scales thus becomes a prerequisite. It is shown here that this fine description of ponds over the Ferlo region (Senegal) can be accomplished by using high-spatial resolution SPOT-5 images. New NDPI and NDTI indices introduced in this paper can thus describe spatio-temporal variability and evolution of small and clustered ponds, with or without vegetation and/or turbid or not, during the rainy season.

Moreover, following recent results by Bâ et al. (2005) for the same region, showing that *Aedes* and *Culex* mosquitoes can be found as far as 500 m from the edges of ponds, a new experimental product or the Zone Potentially Occupied by Mosquitoes (ZPOM) is proposed. As such the ZPOM has then been calculated by applying a 'buffer zone' from the remotely sensed ponds and based upon the mosquitoes flying range (Fig. 7). Interestingly, the displayed ZPOM shows that small ponds distributed in clusters can unexpectedly generate a large potential presence of mosquitoes. In Fig. 7, it is seen that during August 26th, 2003 ponds areas represented ∼1% of the studied zone (i.e., 1703 ha), while the ZPOM reached almost 25% for that same zone (∼49,334 ha). Indeed, contribution of large ponds (larger than 0.5 ha and occupying 1562 ha of the studied area) is of 29,229 ha for the ZPOM. If only clusters of small ponds are considered (less than 0.5 ha and occupying only 141 ha of the studied area), their contribution to the ZPOM is still of 20,105 ha.

It is believed that this new remotely sensed approach of ponds and their characteristics, if properly coordinated with in-situ monitoring and if implemented in close collaboration with entomologists, should facilitate the study of mechanisms involved with RVF diffusion and transmission. This should improve early warning systems linked to vector borne epidemics. African health information systems, agencies and organizations over West Africa will thus have a panoply of additional products in support of appropriate measures to apply in regions under threats. The same applies to other vector borne diseases.

References

Anyamba, A., & Tucker, C. J. (2005). Analysis of Sahelian vegetation dynamics using NOAA-AVHRR NDVI data from 1981−2003. *Journal of Arid Lands*, *63*, 569−614.

Anyamba, A., Linthicum, K. J., & Tucker, C. J. (2001). Climate-disease connections: Rift Valley Fever in Kenya. *Cardernos de Saúde Pública, Rio de Janeiro*, *17*, 133−140.

Bâ, Y., Diallo, D., Fadel Kebe, C. M., Dia, I., & Diallo, M. (2005). Aspects of bioecology of two Rift Valley Fever virus vectors in Senegal (West Africa): *Aedes vexans* and *Culex poicilipes* (Diptera: Culicidae). *Journal of Medical Entomology*, *42*(5), 739−750.

Beaty, B. J., & Marquardt, W. C. (1996). *The biology of disease vectors.* University Press of Colorado.

Bicout, D. (2001). Eléments sur la biologie des vecteurs de RVF. *Rencontre modélisation sur la Fièvre de la Vallée du Rift, Nîmes, 8–9 Février 2001*.

Bonn, F., & Rochon, G. (1996). Précis de télédétection. *Volume 1: Principes et methods* (pp. 311−316). Québec, Canada: Presse de l'Université du Qubec/ AUPELF, ISBN2-7605-0613-4.

Campbell, J. B. (1996). *Introduction to remote sensing* (4nd ed.). New York, USA: Guilford Publications, ISBN1-59385-319-X.

Chevalier, V., Lancelot, R., Thiongane, Y., Sall, B., Diaïté, A., & Mondet, B. (2005). Rift Valley Fever in small ruminants, Senegal, 2003. *Emerging Infectious Diseases*, *11*(11), 1693−1700.

Chevalier, V., Mondet, B., Diaïté, A., Lancelot, R., Fall, A. G., & Ponçon, N. (2004). Exposure of sheep to mosquito bites: possible consequences for transmission risk of Rift Valley Fever in Senegal. *Medical and Veterinary Entomology*, *18*, 247−255.

Diallo, M., Nabeth, P., Bâ, K., Sall, A. A., Bâ, Y., Mondo, M., et al. (2005). Mosquitoes vectors of the 1998–199 outbreak of Rift Valley Fever and other arboviruses (Bagaza, Sanar, Wesselsbron and West Nile) in Mauritania and Senegal. *Medical and Veterinary Entomology, 19*, 119−126.

Fontenille, D., Traoré-Lamizana, M., Diallo, M., Thonnon, J., Digoutte, J. P., & Zeller, H. G. (1998). New vectors of Rift Valley Fever in West Africa. *Emerging Infectious Diseases, 4*, 289−293.

Guyot, G. (1989). Signatures spectrales des surfaces naturelles. Télédétection satellitaire, 5, Col. SAT, Ed. Paradigme, pp 178.

Guyot, G., & Seguin, B. (1988). Possibilités d'utilisation de la télédétection satellitaire en agrométéorologie. *Agronomie, 8*, 1−13.

Jarlan, L., Tourre, Y. M., Mougin, E. P., & Mazzega, P. (2005). Dominant patterns of AVHRR NDVI interannual variability over the Sahel and linkages with key climate signals (1982–2003). *Geophysical Research Letters, 32*, L04701, doi:10.1029/2004GL021841.

Linthicum, K. J., Anyamba, A., Tucker, C. J., Kelley, P. W., Myers, M. F., & Peters, C. J. (1999). Climate and satellite indicators to forecast Rift Valley Fever epidemics in Kenya. *Science, 285*, 397−400.

Mondet, B., Diaïté, A., Ndione, J. A., Fall, A. G., Chevalier, V., Lancelot, R., et al. (2005). Rainfall patterns and population dynamics of *Aedes* (*Aedimorphus*) *vexans arabiensis*, Patton 1905 (Diptera: Culicidae), a potential vector of Rift Valley Fever virus in Senegal. *Journal of Vector Ecology, 30*, 102−106.

Mondet, B., Diaïté, A., Fall, A. G., & Chevalier, V. (2005). Relations entre la pluviométrie et le risque de transmission virale par les moustiques: cas du virus de la Rift Valley Fever (RVF) dans le Ferlo (Senegal). *Environnement, Risques et Santé, 4*, 125−129.

Moron, V. (1994). Guinean and Sahelian rainfall anomaly indices at annual and monthly scales (1933–1990). *International Journal of Climatology, 14*, 325−341.

Ndione, J-A., Besancenot, J-P., Lacaux, J-P., & Sabatier, Ph. (2003). Environnement et épidémiologie de la fièvre de la vallée du Rift (FVR) dans le bassin inférieur du fleuve Sénégal. *Environnement, Risques et Santé, 2*, 1−7.

Nicholson, S. E. (1979). Revised rainfall series for the West African subtropics. *Monthly Weather Review, 107*, 620−623.

Porphyre, T., Bicout, D. J., & Sabatier, P. (2005). Modelling the abundance of mosquito vectors versus flooding dynamics. *Ecological Modelling, 183*, 173−181.

Puech, C. (1994). Plans d'eau sahéliens et imagerie SPOT: inventaire et évaluation des capacités d'exploitation. *Colloque international "Eau, environnement et développement" Colloque de l'Institut des Relations Interuniversitaires avec la Mauritanie (IRIM)-Université de Nice/Sophia-Antipolis et de l'Institut Mauritanien de la Recherche Scientifique (IMRS), Nouakchott, 20–22 mars 1994* (pp. 68−83).

Robin, M. (1995). *La télédétection, des satellites aux systèmes d'information géographiques Nathan Université Edition, Paris, France* (pp. 30−32)., ISBN209 190293-4.

Rouse, J. W., Haas, R. H., Schell, J. A., & Deering, D. W. (1973). Monitoring vegetation system in the Great Plains with ERTS. *Third "Earth Resources Technology Satellite" symposium, Vol. 1.* (pp. 309−317) Washington D.C.: NASA SP353.

Thomson, M. C., Doblas-Reyes, F. J., Mason, S. J., Hagedorn, R., Connor, S. J., Phindela, T., et al. (2006). Malaria early warnings based on seasonal climate forecasts from multi-model ensembles. *Nature, 439*, 576−579.

Traoré-Lamizana, M., Fontenille, D., Diallo, M., Bâ, Y., Zeller, H. G., Mondo, M., et al. (2001). Arbovirus surveillance from 1990 to 1995 in the Barkedji Area (Ferlo) of Senegal, a possible natural focus of Rift Valley Fever virus. *Journal of Medical Entomology, 38*, 480−492.

Tucker, C. J. (1979). Red and photographic infrared linear combinations for monitoring vegetation. *Remote Sensing of Environment, 2*, 127−150.

Tucker, C. J., & Nicholson, S. E. (1999). Variations in the size of the Sahara Desert from 1980–1997. *Ambio, 28*, 587−591.

Verbyla, D. L. (1995). *Satellite remote sensing of natural resources.* Boca Raton, USA: Lewis Publishers/CRC Press LLC, ISBN1566701074 224 pp.